*Journal of Fluids and Structures* (1997) **11,** 893–907

# FLOW ABOUT CYLINDERS WITH SURFACE PERTURBATIONS

H. H. NIGIM* AND S. M. BATILL†

*Department of Mechanical Engineering, Birzeit University, P. O. Box 14 Birzeit, Palestine

†Hessert Center for Aerospace Research, University of Notre Dame Notre Dame, Indiana, U.S.A.

(Received 3 December 1996 and in revised form 19 August 1997)

An experimental study of circular cylinders with equally spaced two-dimensional surface perturbations in a uniform flow at Reynolds number of $3 \times 10^4$ and very low free-stream turbulence is presented. The investigation concentrates on how the major flow characteristics are influenced by the geometry of the perturbations, their distribution and spacing, and orientation relative to the uniform flow. Measurements of body-surface pressures, vortex-formation length, spacing between the shear layers, vortex-shedding frequency and mean and fluctuating velocities within the wake as well as the drag force are presented. It is found that the drag coefficient and Strouhal number vary significantly with the location of the perturbations. The influence of the surface perturbations on the major flow characteristics are described and correlated with the near-body flow field. 

## 1. INTRODUCTION

ARISING FROM the increasing practical importance of bluff-body aerodynamics, a substantial amount of data has been accumulated by researchers on the two-dimensional flow around smooth-surface bodies. Experiments have been performed on smooth circular cylinders over a wide range (from $10^3$ to $10^7$) in the Reynolds number, Re, where Re is based on the cylinder diameter, $D$, and the free-stream velocity, $U$. In low-turbulence streams, the flow field undergoes some dramatic changes, and three regimes can be identified: sub-critical for $1500 < \mathrm{Re} < 2 \times 10^5$, super-critical for $\mathrm{Re} > 2 \times 10^5$, and post-critical for $\mathrm{Re} > 10^7$. The nature of the transition from sub-critical to super-critical, and the transition from super-critical to post-critical, has been discussed by Basu (1985). For the range of Re from about $10^4$ to at least $2 \times 10^5$, where the point of transition is close to the point of separation and the major portion of the free shear layer is turbulent, the flow field is nearly independent of Re. The actual range of Re for each regime is sensitive to factors such as free-stream turbulence and model geometry, including length-to-diameter ratio, model end conditions, alignment of the model axis and surface perturbations. Due to the large number of parameters, most experiments concentrate on varying one or two parameters.

The desire to explore the effect of surface perturbations and to correlate the results in a systematic way is frustrated by the fundamental difficulty that the number of parameters describing perturbations is extraordinarily large, owing to the great diversity of geometric forms. A variety of perturbation types have been used in existing measurements on flow

0889–9746/97/080893 + 15 $25.00/fl970116 

over circular cylinders. In many studies sandpaper or distributed surface roughness were adapted to simulate surface perturbation. Using a number of different emery papers, Achenbach (1971) found that large surface perturbations may cause immediate transition to turbulence and decrease in $C_d$ from 1·2 to 0·7 at Reynolds numbers as low as $6 \times 10^4$. He has concluded that the formation of laminar-separation turbulent-reattachment bubbles is responsible for the low values of the drag coefficient $C_d$ which occur at the beginning of the super-critical regime. Above sub-critical regimes, both Szechenyi (1975) and Buresti (1981) examined the influence of the surface perturbations. To perturb the surface of the cylinder, Szechenyi used calibrated spherical beads, while Buresti used different types of standard commercial emery cloth.

For certain applications, the surface perturbations can be classified according to their effects on the flow as well as their geometry. Perry *et al.* (1969) have shown that the flow field resulting from arrays of two-dimensional surface perturbations depends on their size, the spacing between the perturbations, and the surface curvature. In their experimental study, turbulent boundary layers were developed over the arrays in both zero and adverse pressure gradients. The spacing-to-height ratio of the surface perturbations is used to classify these arrays into *k*- and *d*-type arrays, as shown in Figure 1. Practically, the *k*-type array is the distribution of surface perturbations where vortices are shed into the flow from the space between the perturbations. This is distinct from the *d*-type array in which the small spaces can be regarded as cavities in which steady local vortices form (Najim & Ghoniem 1992).

The motivation for the present investigation has been provided by the complex-flow physics associated with the flow about cylinders with surface perturbations. This paper describes detailed measurements of the flow field about circular cylinders with equally spaced two-dimensional surface perturbations at a Reynolds number of $3 \times 10^4$ and very low free-stream turbulence. The results concentrate on how the major flow characteristics, such as pressure coefficient, $C_p$, vortex formation length, $L$, spacing between the shear layers, $b$, and vortex-shedding frequency, $f$, as well as pressure drag, are influenced by the geometry of the perturbations, their distribution and spacing.

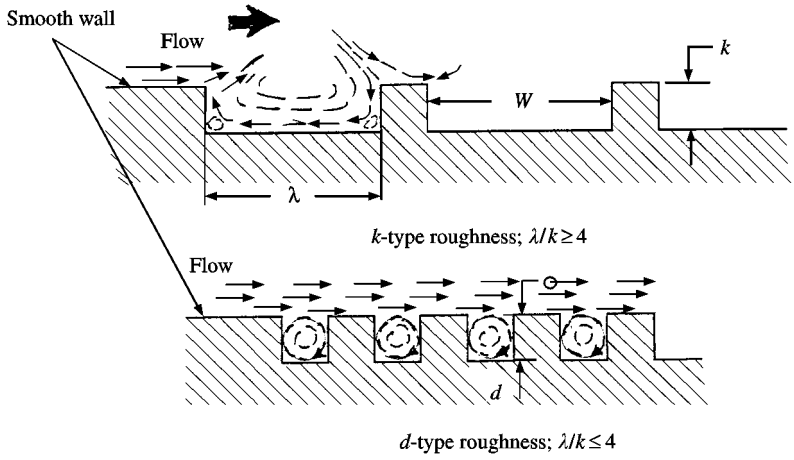


Figure 1. Geometry of rough wall used by Perry *et al.* (1969); *k*- and *d*-type roughness.

Previous work by Nebres (1992) using a single spanwise surface perturbation helped provide initial insight into this problem. With such a simple geometry it was observed that the vortex-shedding frequency, $f$, is a function of the surface perturbation angular position, $\theta$, which has a significant influence on the boundary layer and thus the location of separation.

## 2. FLOW CONFIGURATION, EXPERIMENTAL METHODS AND PROCEDURES

This section briefly describes the technique for the aerodynamic measurements, the complete details of which can be found in Nebres (1992). The experiments were conducted at Hessert Center for Aerospace Research, University of Notre Dame, U.S.A. An in-draft, sub-sonic wind tunnel was used. It has a convergent section with contraction ratio of 20·6 : 1 based on the area, and a set of 12 anti-turbulence screens ensures a uniform velocity profile at the entrance to the square (610 mm × 610 mm) test-section and a low turbulence level of about 0·05%. The flow velocity was monitored through a digital differential manometer via a Pitot-static tube placed in flow.

For the major part of the investigation, perturbations with circular cross-section and a diameter, $d$, of 4 mm were added to a baseline circular cylinder with a diameter, $D$, of 44·5 mm and thus the ratio of $d/D$ was 0·09. A second model with a $d/D$ of 0·07 was also used for a limited number of tests. The spacing-to-height ratio, $S/d$, was varied in an attempt to model both $k$- and $d$-type arrays of surface perturbation. End-plates with sharp leading edges were used to isolate the flow over the model from the boundary layers of the tunnel walls. In all tests, circular end-plates of 325 mm diameter were used, except during the force–balance measurements where rectangular end-plates of 600 mm (streamwise) by 235 mm were used. All measurements were made at the mid-span of the tested models which have aspect ratios about 10 based on the area. According to Fox & West (1990), the data are considered free from end effects. The models were positioned normal to the uniform free-stream, and the orientation of the perturbations was varied by rotating the model through the angle $\theta$ as shown in Figure 2. The angle $\theta$ is referred to as the incidence angle in this paper. The ratio of the arc length or spacing between the surface perturbations, $S$, and the perturbation diameter is also indicated in Figure 2. The estimated uncertainty of angular positioning of the model was $\pm 0{\cdot}50^{\circ}$.

Surface-pressure measurements were only carried out for the $d/D = 0{\cdot}09$ models. A total of 48 pressure taps were connected to pressure instrumentation outside the tunnel via Tygon tubes. This instrumentation was coupled to the data acquisition system which acquired 250 samples at 4 ms per sample, and then averaged to obtain time-averaged pressure coefficients, $C_p$. The uncertainty in the pressure coefficient, for a confidence level of 95%, was estimated to be $\pm 0{\cdot}02$.

To measure the total mean drag force, $F_d$, an external platform balance was used. The platform balance was located on the top of the test-section, as shown in Figure 3. The clearance between the ends of the 464 mm span model and each end-plate was about 1 mm. Tests were performed with the 1 mm clearance filled with light machine oil. Such arrangements made it possible to exclude the force on the end-plates from the drag measurements. For each set of data the balance was calibrated, and at least 10 000 samples were obtained and averaged for each measurement. The uncertainty for the drag measurements are $\pm 0{\cdot}015$ N. The drag data are presented in terms of the dimensionless mean drag coefficient $C_d$. Schlichting (1968) defined the mean drag coefficient based on the free-stream dynamic

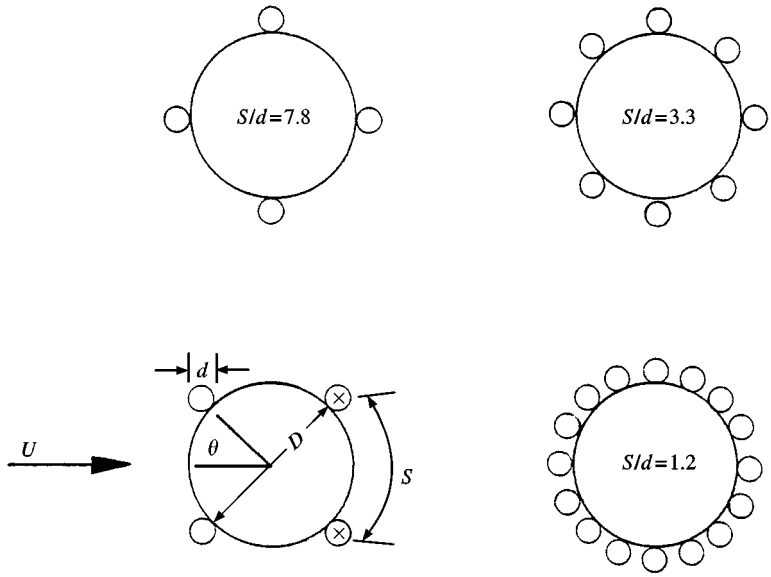


Figure 2. Schematic of cross-sections for various models for $d/D = 0{\cdot}09$.

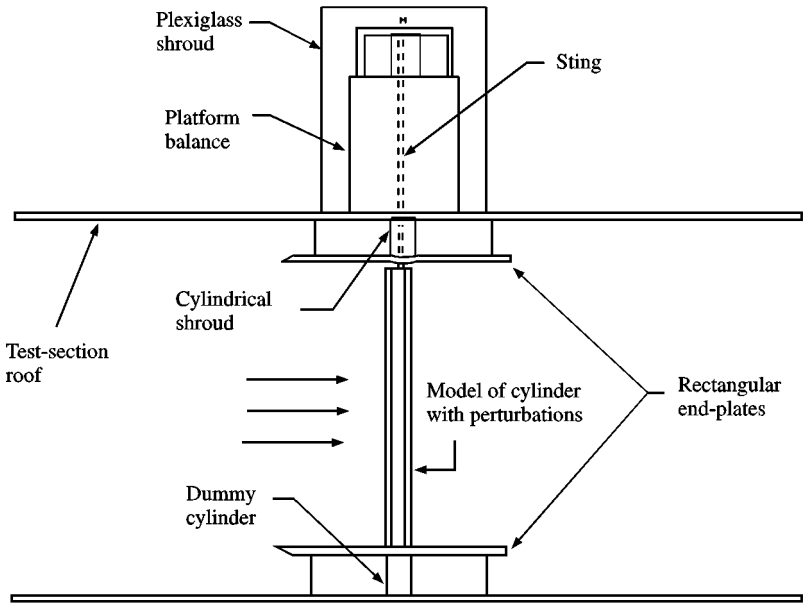


Figure 3. Details of test model mounted across tunnel test-section and location of platform balance.

pressure as $C_d = 2F_d/A\rho U^2$, where $A$ is the smooth-cylinder frontal area(the cylinder length times $D$), $\rho$ is the fluid density and $U$ is the upstream uniform velocity.

When a body is tested in a finite flow field, the drag force has to be corrected for wind-tunnel blockage effects. These effects, which arise from the solidity of the body and

from the effective solidity of the wake, cause velocities near the body to be higher than they would be in an infinite stream. The effect on the drag of isolated bodies in a uniform stream is usually assumed to be similar to a simple increase in the approach velocity of the corresponding unbounded stream. In the present investigation, where the characteristics of the flow separation and reattachment play a large part in determining the drag, the applicability of this concept is in doubt. Therefore, no correction was applied to the present results. However, the conclusions drawn on the drag coefficient are unlikely to be invalidated by blockage effects.

Both formation-length measurements and wake velocity profile surveys were conducted using a single wire, hot-wire anemometry system. Here, as was first used in Bloor (1963), the formation length, $L$, is defined as the location where the value of the r.m.s. velocity fluctuating at twice the shedding frequency is at its maximum on the wake axis. For each measuring position, at least a sample of 1024 data points was obtained at a sampling rate of 100 Hz. The hot-wire data was filtered and for the formation-length measurements the r.m.s. of the AC coupled hot-wire signal at twice the shedding frequency was computed. To obtain the time-averaged velocity the samples were converted to velocity using a calibration developed in a tunnel without cylinder and the Pitot-static probe. The uncertainty in the formation length measurement is estimated to be $\pm 0{\cdot}1\,D$.

The hot-wire anemometer system was used for the measurements of the vortex-shedding frequency. The analog hot-wire signal was high-pass filtered at 0·1 Hz by an intelligent Flow Analyzer (TSI-IFA 100) to eliminate the DC component. The analog signals were then acquired by a Spectral Dynamics signal analyzer (Scientific Atlanta SD380). To avoid the noise from the turbulent vortex street, it was necessary to locate the probe at $2\,D$ laterally from the cylinder axis and $1{\cdot}5\,D$ from the cylinder surface, where $D$ is the diameter of the cylinder without the presence of surface perturbations. The estimated uncertainty in the shedding frequency is $\pm 0{\cdot}2$ Hz.

## 3. RESULTS, DISCUSSION AND MODELLING

All the results presented in the paper are for a Reynolds number of $3 \times 10^4$ based upon the base cylinder diameter, $D = 44{\cdot}5$ mm, and the free-stream velocity, $U = 10$ m/s. At this Reynolds number the point of transition is close to the point of separation for the smooth cylinder and the major portion of the free-stream layer is turbulent. This Reynolds number is experienced in many engineering applications. Under such experimental conditions, a substantial amount of data has been accumulated by investigators on two-dimensional smooth-surface cylinders. In the present study, the smooth-cylinder data is used as a reference case for the rest of the experiments and to verify the experimental procedures.

The distributions of mean surface-pressure coefficient, $C_p$, for a perturbed cylinder with a spacing-to-height ratio, $S/d$, equal to 7·8, are presented in Figure 4 with $\theta$ ranging from 0 to 90°. Positions on the surface of the model are indicated using the angle $\theta$ which is measured clockwise from the forward stagnation point on the smooth cylinder. (This is the model with four evenly spaced perturbations). The mean surface pressure coefficients in the vicinity of the "forward-facing" perturbations are similar to those obtained by Nebres (1992) for a single perturbation. Before and after the perturbations, there are regions of constant pressure that vary with the orientation angle and the location of each perturbation. The figure shows that the distributions of the mean pressure coefficient depend on the perturbation angular positions. The constant pressure region after a perturbation can have

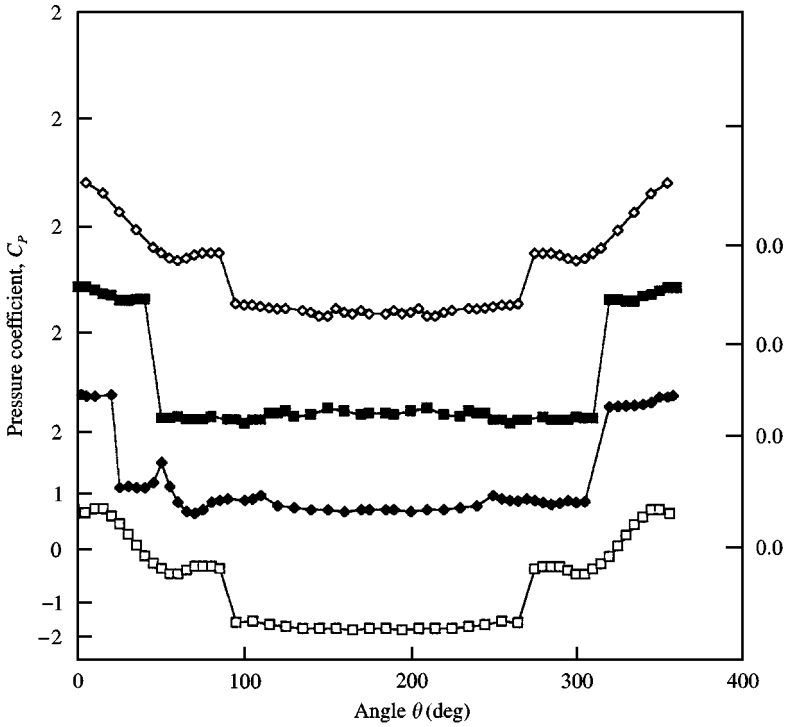


Figure 4. Pressure distribution around the perturbed cylinder at different angle of incidence. $\theta$: —□—, $\theta = 0$; —◆—, $\theta = 22{\cdot}5°$; —■—, $\theta = 45°$; —◇—, $\theta = 90°$. $S/d = 7{\cdot}8$, $D/d = 0{\cdot}09$.

values as low as $-1{\cdot}5$, while the base-pressure region $C_{pb}$ (defined as the average of the nearly constant pressure coefficients in the wake region) ranges from $-1$ to $-1{\cdot}5$.

The four cases presented in Figure 4 help to illustrate the complexity of this two-dimensional flow. From the present measurements and Nebres (1992) detailed flow visualization measurements for a single perturbation, certain comments about the flow-field and boundary-layer separation and reattachment process can be made. For $\theta = 0°$ there is a perturbation directly aligned with the free stream. The flow separates from the surface of the perturbation, then reattaches, the flow accelerates and $C_p$ decreases, until another separation occurs forward of the perturbations located at $\pm 90°$ at a $\theta$ approximately $\pm 60°$. Recirculation occurs in the region forward of this second perturbation and shear layer impinges on the perturbation and final separation occurs from the perturbation and the wake is formed.

When $\theta = 22{\cdot}5°$, there is a perturbation located at $+22{\cdot}5°$ and $-67{\cdot}5°$. For the perturbation located at $+22{\cdot}5°$, separation occurs forward of the perturbation and a bubble forms aft as the transitioned free-shear layer reattaches. The flow then accelerates and separation occurs at approximately $\theta = 80°$. There is a significant separated region forward of the perturbation located at $-67{\cdot}5°$, and the pressure aft of that perturbation is equal to the base pressure on the cylinder. For the $\theta = 45°$ case, there are separated regions forward of the perturbations, which are symmetric, and no reattachment downstream.

The variation of $C_d$ with the angle of incidence $\theta$ is shown in Figure 5. In the figure the spacing-to-height ratio, $S/d$, is varied in angular dimensions to model both $k$-type arrays

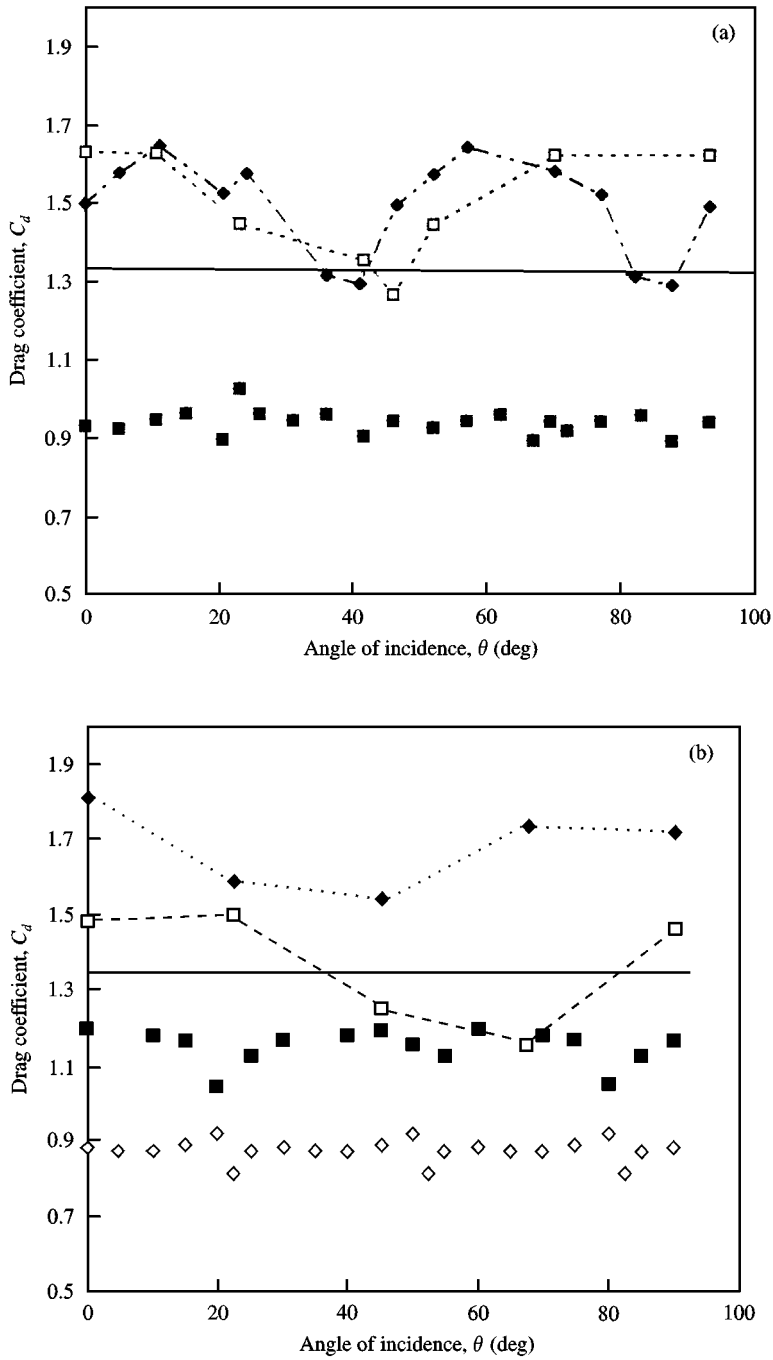


Figure 5. Measurements of drag coefficient, $C_d$ versus the angle of incidence, $\theta$, for cylinders of different perturbation density, $S/d$. (a) For $d/D = 0{\cdot}09$; ——, smooth cylinder; □, $S/d = 7{\cdot}8$; ◆ $S/d$ 3·3; ■, $S/d = 1{\cdot}2$. (b) For $d/D = 0{\cdot}07$; □, $S/d = 10$; ◆, $S/d = 6{\cdot}5$; ■, $S/d = 2{\cdot}75$ ◇, $S/d = 0{\cdot}9$; ——, smooth cylinder.

and $d$-type arrays of surface perturbations. Figure 5(a, b) presents results for the models with diameters ratio of $d/D = 0{\cdot}09$ and $0{\cdot}07$, respectively. The results suggest that the demarcation between $k$- and $d$-type arrays is about three. The figure shows that, if $S/d > 3$ ($k$-type arrays), the maximum value of $C_d$ can be as high as 1·75. The variations of $C_d$ with the angle of incidence is periodic as suggested by the regular spacing of the perturbations. Figure 5(a) indicates that at $S/d = 3{\cdot}3$, a change in $\theta$ of 45° produces an identical geometry, but at $S/d = 7{\cdot}8$ a change of 90° is required. In the case of $S/d < 3$ ($d$-type arrays) the drag coefficient is almost constant and the variation of $C_d$ with $\theta$ is less obvious. When $S/d < 3$, the mean value of $C_d$, which depends on both $S/d$ and $d/D$, is always less than that obtained for smooth-surface cylinder. There is a similar variation of the inverse of the vortex-shedding frequency, $1/f$, with the angle of incidence $\theta$.

The frequency data is non-dimensionalized in the form of a Strouhal number, $\mathrm{St} = fD/U$. Typical values of the ratio of perturbed cylinder Strouhal number, St, to the smooth cylinder Strouhal number, $\mathrm{St}_0$, with orientation for all tested models are illustrated in Figure 6(a, b). For smooth-surface circular cylinders and over a wide range of Reynolds number $10^3 < \mathrm{Re} < 10^5$, the value of Strouhal number is almost constant, $\mathrm{St}_0 = 0{\cdot}2$. This value depends on the free-stream turbulence levels as well as length/diameter ratio. For perturbation density $S/d > 3$, the Strouhal number varies significantly with the angle of incidence $\theta$, assuming multiple maxima and minima. The maximum Strouhal number observed during this study, which depends on both $S/d$ and $\theta$, is about 160% of the smooth-surface cylinder, while the minimum value is about 80%. Figure 6 shows that at $S/d < 3$ ($d$-type arrays), the Strouhal number is almost constant and is always higher than that obtained for a smooth-surface cylinder. Also any variation of St with $\theta$ is less obvious for this case.

In Figures 5 and 6, there is similarity in the variation with cylinder orientation of these two important parameters with $S/d > 3$. However, in Figures 5(b) and 6(b), a difference in the orientations associated with the maximum and minimum values can be observed. This may be due to the difficulties arising from determining the exact position of perturbation angle of incidence $\theta$ of the model relative to the flow, especially in the region $\theta = 45°$. Nebres (1992) reported that the separation bubble behind the perturbation is collapsing at $\theta = 43°$. In this case, a 50% change in Strouhal number and the drag coefficient could be achieved, simply by changing $\theta$ by 1°.

Because of the complex nature of the wake dynamics, including the formation of organized vortex systems and the lack of knowledge of the link between wake and separation conditions, realistic theoretical models of the separated flow past a bluff body have included some empiricism. The Strouhal numbers, St, are plotted against the drag coefficient, $C_d$, in Figure 7. The figure demonstrates the relationship between $C_d$ and St, and from which the following linear approximation for the drag coefficient as a function of Strouhal number is proposed:

$$C_d = 3{\cdot}3 - 10(\mathrm{St}). \tag{1}$$

Figure 7 shows, in addition to the present data, a comparison between equation (1) and the empirical relationship, for smooth-surface cylinders, first reported by Hoerner (1965), $\mathrm{St} = 0{\cdot}21/(C_d)^{3/4}$. It appears that, only for $S/d < 3$ ($d$-type arrays), Hoerner's relationship gives a rather satisfactory agreement with the data obtained. Hence, equation (1) can be used to determine the points of maximum and minimum $C_d$ with an accuracy of $\pm$ 15%. It also confirms the idea of the existence of a link between the drag coefficient of a bluff body

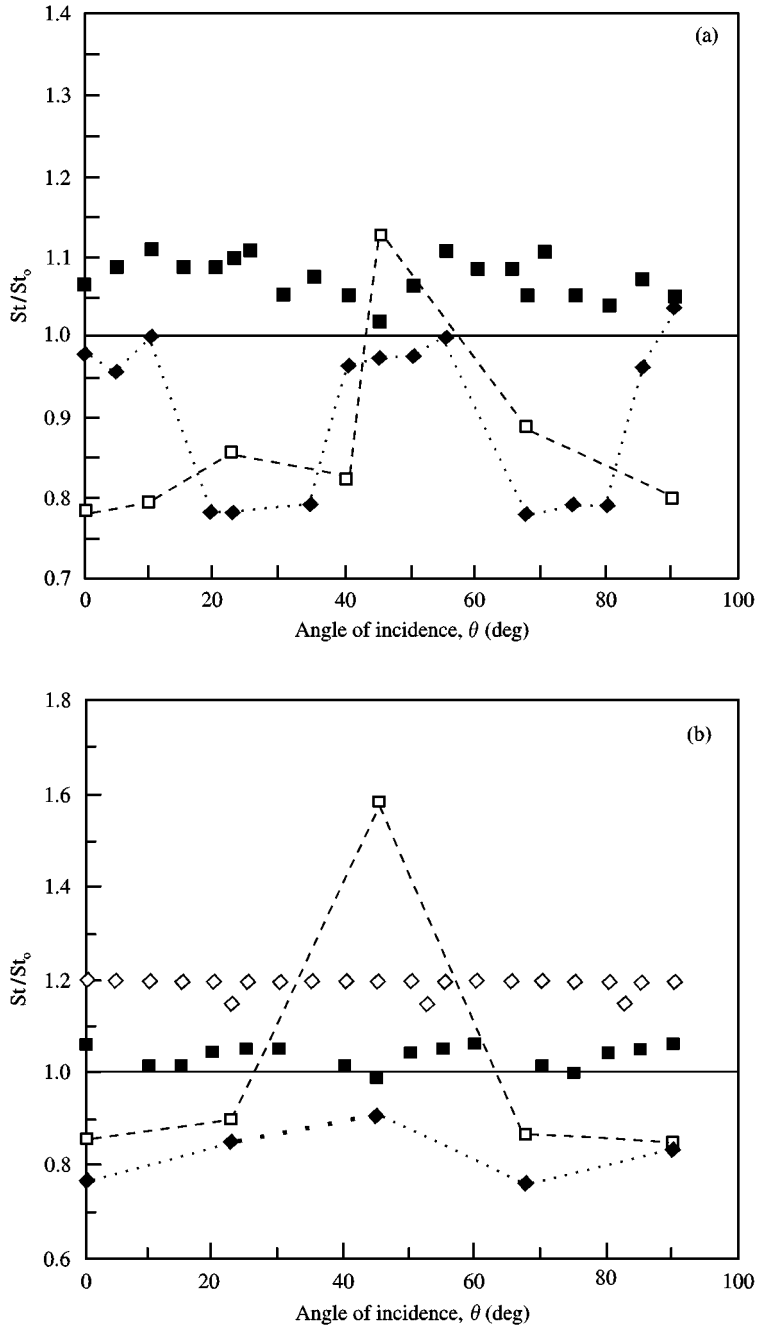


Figure 6. Strouhal number ratio, $St/St_0$ versus angle of incidence, $\theta$, for cylinders with equally spaced surface perturbations. (a) For $d/D = 0{\cdot}09$; □, $S/d = 7{\cdot}8$; ◆, $S/d = 3{\cdot}3$; ■, $S/d = 1{\cdot}2$; ——, smooth cylinder. (b) For $d/D = 0{\cdot}07$: □, $S/d = 10$; ◆, $S/d = 6{\cdot}5$; ■, $S/d = 2{\cdot}75$; ◇, $S/d = 0{\cdot}9$; ——, smooth cylinder.

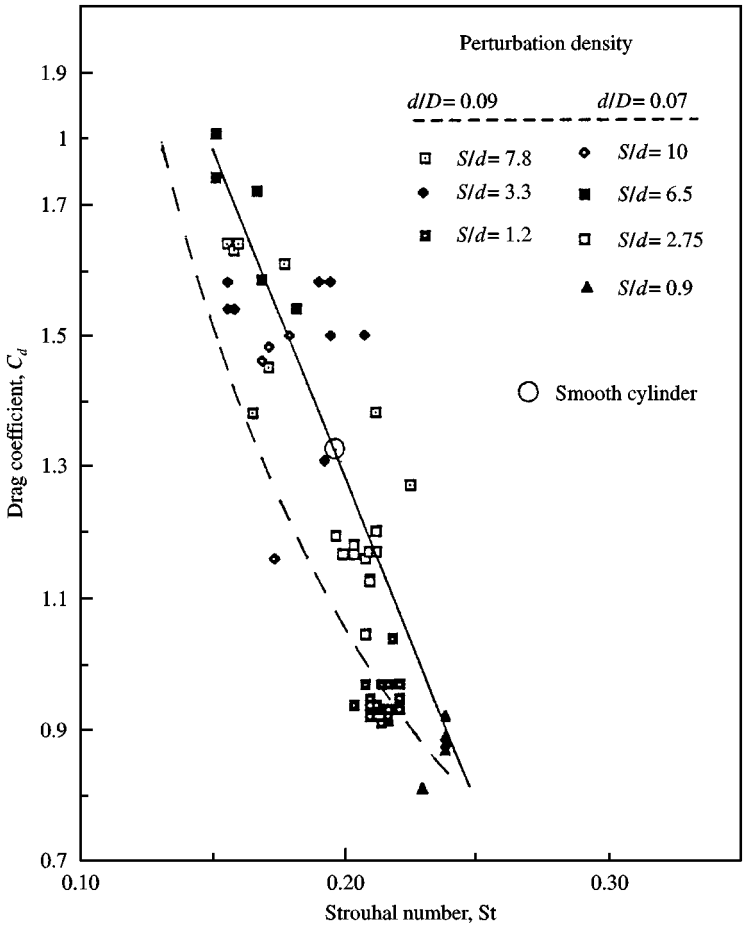


Figure 7. Drag coefficient, $C_d$, versus Strouhal number, St, for cylinders with equally spaced surface perturbations. Comparison between experimental data points and: ——, equation (1); – – –, Hoerner (1965).

and the corresponding Strouhal number, as suggested by many researchers (Hoerner 1965; Griffin 1978; Roshko 1993).

In order to acquire some additional insight into the flow field about the perturbed cylinders, measurements in the region of vortex formation approximately four or five diameters behind the models were carried out, Gerrard (1966) has reported that the wake-formation region behind a circular cylinder can be used as a relevant length scale. In the present investigation, the formation length is equivalent to the distance downstream from the cylinder where the free shear layer first crosses the wake centreline. Experimentally, it is the location where the r.m.s. of the velocity fluctuations at twice the shedding frequency is maximum. Bearman (1967) noticed that correlation existed between the product of the Strouhal number and the drag, $\mathrm{St}C_d$ and the base pressure. The wake development has been correlated with the near-body flow field and thus the base pressure. Figure 8 shows the variation of the non-dimensionalized formation length $L/D$ with $\mathrm{St}C_d$ in linear-logarithmic coordinates. A regression analysis shows that the following relationship

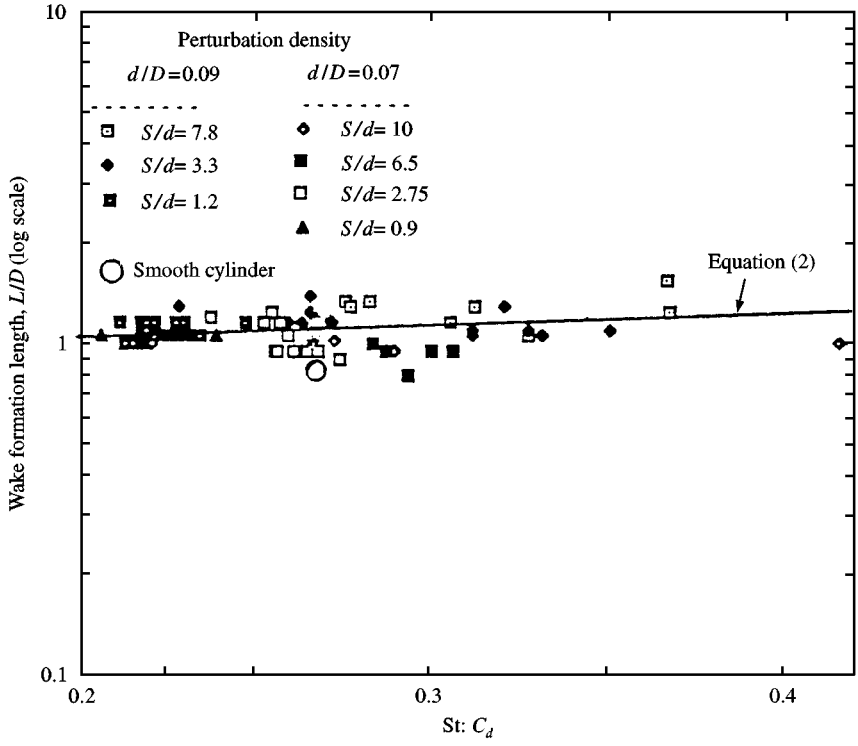


Figure 8. Dependence of the non-dimensional formation length, $L/D$, on St $C_d$ for cylinders with equally spaced surface perturbations.

gives the best fit of the data:

$$\mathrm{Log_e}(L/D) = 0{\cdot}1 + 0{\cdot}5(\mathrm{St}C_d). \tag{2}$$

As a measure of the wake width, the shear layer spacings were also obtained using a conditional averaging measurement developed by Nebres (1992). This technique satisfies the assumptions of Roshko (1955), that the shear layers be parallel at the downstream location where the measurement is made. Thus, wake velocity profiles were measured at different streamwise stations to determine where the shear layers become parallel. Figure 9 illustrates the correlation between the wake width $b/D$ and the base-pressure parameter $k = U/U_S$, where $U_S$ is the velocity of the irrotational flow at separation. This is based upon the observation that the difference between the pressure just after separation and the pressure at $\theta = 180^\circ$ from the stagnation point is insignificant. For the present study the surface pressure at $\theta = 180^\circ$ was used to evaluate the base pressure parameter $k$. In addition, Figure 9 contains the results from the "notched hodograph theory" obtained by Roshko (1954). The disagreement between the experimental data and Roshko's theory may well be related to the fact that the theory is not applicable when the separation point is on the back side of the model, as it has been observed to be during the present investigation.

Finally, the current results were used to determine whether certain proposed universal wake numbers can be used to define certain characteristics of flow about circular cylinders with large-scale surface perturbations. Most of the proposed universal wake numbers are,

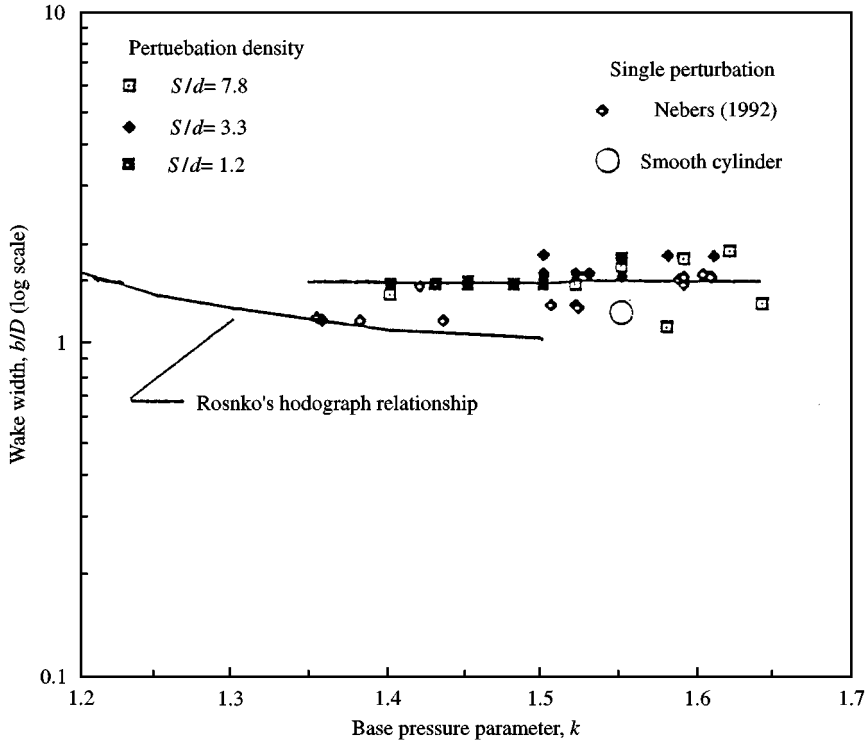


Figure 9. Variation of base pressure parameter, $k$, with wake width, $b/D$, for cylinders with equally spaced surface perturbations.

essentially, modified Strouhal numbers. This is the case for the numbers proposed by Roshko (1955), Bearman (1967), Griffin (1978) and Nebres (1992). The results demonstrated the need for improved understanding of the mechanism which couples the forces acting on a bluff body and the vorticity shed in its wake. The current results indicated that only for $S/d < 3$ was Griffin's number found to correlate the experimental data with reasonable accuracy, as shown in Figure 10.

## 4. CONCLUSIONS

The results presented in this study have illustrated some interesting features of the flow field about circular cylinders with relatively large, equally spaced, two-dimensional surface perturbations at a Reynolds number of $3 \times 10^4$. These experiments were performed at a very low free-stream turbulence level. This study was performed in order to quantify a number of characteristics of this important fluid–structure interaction. These included details on the surface-pressure distribution, drag force, and wake characteristics. The following conclusions can be drawn from these experiments.

(i) In the range of the spacing-to-height ratio, $S/d$, covered by the present investigation, it appears that surface perturbations may be broadly divided into $k$- and $d$-type arrays, using the classification defined by Perry *et al.* (1969). The demarcating value of $S/d$ is approximately 3 for perturbations on circular cylinders.

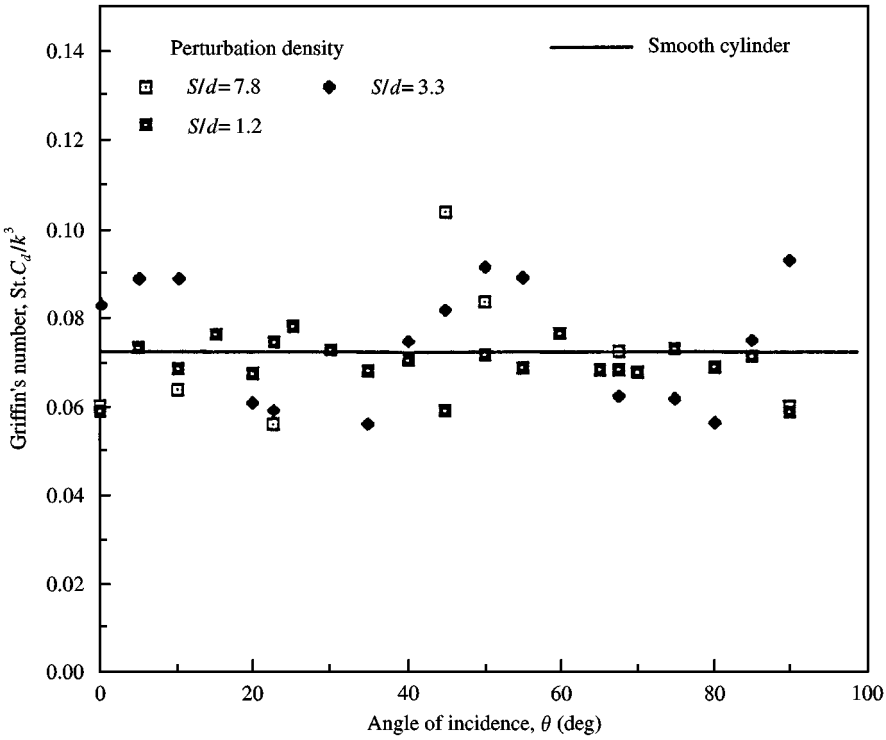


Figure 10. Griffin's number versus the flow angle of incidence, $\theta$, for cylinders with equally spaced surface perturbations.

(ii) For the cases where $S/d > 3$ and for $k$-type arrays, a small variation in the angle of incidence $\theta$ can lead to significant variations in the drag coefficient, and the vortex-shedding frequency. These variations can be correlated to the periodicity associated with the perturbation positions relative to the free-stream.

(iii) When $S/d < 3$, for $d$-type arrays the mean value of $C_d$ is almost constant and less than that obtained for a smooth-surface cylinder. For these cases, the Strouhal number is also nearly constant and on the average higher than that associated with a smooth cylinder at this Reynolds number.

(iv) The effects of surface perturbations on both the mean drag and the vortex-shedding frequency are the result of an apparent shift in the transitional regions to a lower Reynolds number. The insensitivity to the small variation of the ratio $d/D$ considered here can be explained in that the cavity flow is primarily influenced by the surface curvature of the cylinder and not the absolute height of the perturbations.

(v) The drag coefficient $C_d$ and Strouhal number St are correlated by a simple empirical relationship [equation (1)]. The relationship demonstrates the existence of a link between the drag coefficient for this bluff body and the vortex-shedding frequency in its wake. The existence of this type of correlation is important when attempting to model the complex flow about circular cylinders with surface perturbations.

(vi) The drag coefficients, $C_d$, wake formation length, $L$, and the Strouhal number, St are also correlated, and an empirical relationship has been developed [equation (2)]. This correlation appeared be more consistent for the $d$-type arrays.

(vii) The wake width was relatively insensitive to variations in the base pressure on the cylinder over the wide range of base pressures achieved for the various perturbations and orientations tested as part of this study. On average, the measured wake width was larger than that for the smooth cylinder.

(viii) Attempts to use the current measurements to evaluate the applicability of a number of universal wake numbers was not particularly successful. Only the Griffin number appeared to provide a reasonable correlation for the *d*-type arrays.

Finally, the study illustrates some of the challenges associated with experimental investigations of this class of bodies. The large number of potential surface perturbations and associated distributions pose a daunting challenge. Understanding the complex interaction between the boundary-layer development, which is so significantly altered by the perturbations, and the wake development is central to the development of useful predictions for engineering applications.

## ACKNOWLEDGEMENTS

The first author is grateful for the hospitality and cooperation extended to him by the Hessert Center for Aerospace Research, University of Notre Dame. Also, the funding support by the Fulbright Foundation is gratefully acknowledged.

## References

Achenbach, E. 1971 Influence of surface roughness on the cross-flow around a circular cylinder. *Journal of Fluid Mechanics* **46,** 321–335.

Basu, R. I. 1985 Aerodynamic forces on structures of circular cross-section. Part 1: model-scale data obtained under two-dimensional conditions in low turbulence streams. *Journal of Wind Engineering and Industrial Aerodynamics* **21,** 273–294.

Bearman, P. W. 1967 On vortex street wakes. *Journal of Fluid Mechanics* **28,** 625–641.

Bloor, M. S. 1963 The transition to turbulence in the wake of a circular cylinder. *Journal of Fluid Mechanics*, **19,** 290–304.

Buresti, G. 1981 The effect of surface roughness on the flow regime around circular cylinder. *Journal of Wind Engineering and Industrial Aerodynamics* **8,** 105–114.

Fox, T. A. & West, G. S. 1990 On the use of end plates with circular cylinders. *Experiments in Fluids* **9,** 237–239.

Gerrard, J. H. 1966 The mechanics of the formation region of vortices behind bluff bodies. *Journal of Fluid Mechanics* **25,** 401–413.

Griffin, O. M. 1978 A universal number for the locking-on of vortex shedding to the vibrations of bluff cylinders. *Journal of Fluid Mechanics* **85,** 591–606.

Hoerner, S. F. 1965 *Fluid Dynamic Drag.* Published by the author, Brick Town, NJ: S. F. Hoerner.

Kline, S. J. & Mclintock, F. A. 1953 Describing uncertainties in single sample experiments. *ASME Journal of Mechanical Engineering* **17,** 3–11.

Najim, H. A. & Ghoniem, A. F. 1992 Numerical simulation of the convective instability in a dump combuster. *AIAA Journal* **29,** 911–919.

Nebres, J. V. 1992 A study of wake similarity and vortex formation for two-dimensional bluff-bodies. Ph.D. thesis, Department of Aerospace and Mechanical Engineering, University of Notre Dame, U.S.A.

Perry, A. E., Schofield, W. H. & Joubert, P. N. 1969 Rough wall turbulent boundary layers. *Journal of Fluid Mechanics* **37,** 383–413.

Roshko, A. 1954 A new hodograph for free-streamline theory. NACA Technical Note T.N. 3168.

Roskho, A. 1955 On the wake and drag of bluff bodies. *Journal of the Aeronautical Sciences*, **22,** 124–132.

ROSHKO, A. 1993 Perspectives on bluff body aerodynamics, *Journal of Wind Engineering and Industrial Aerodynamics* **49,** 79–100.
SCHLICHTING, H. 1968 *Boundary Layer Theory*, 6th edn. New York: McGraw Hill.
SZECHENYI, E. 1975 Supercritical Reynolds number simulation for two-dimensional flow over circular cylinders. *Journal of Fluid Mechanics* **70,** 529–542.

## APPENDIX: NOMENCLATURE

| | |
|---|---|
| $A$ | smooth cylinder frontal area |
| $b$ | wake width |
| $C_d$ | mean drag coefficient, equal to $2F_d/A\rho U^2$ |
| $C_p$ | mean pressure coefficient, equal to $P - P_\infty/q_\infty$ |
| $C_{pb}$ | base pressure coefficient |
| $D$ | cylinder diameter |
| $d$ | diameter of surface perturbations |
| $F$ | aerodynamic force component |
| $F_d$ | total mean drag force |
| $f$ | vortex-shedding frequency |
| $f_0$ | cylinder vortex-shedding frequency |
| $k$ | base-pressure parameter, equal to $1 - C_{pb}$ |
| $L$ | vortex-formation length |
| $P$ | mean pressure on cylinder surface |
| $P_\infty$ | free-stream static pressure |
| $q_\infty$ | free-stream dynamic pressure |
| $S$ | spacing between surface perturbations |
| St | Strouhal number |
| $U$ | free-stream velocity |
| $\theta$ | angular position of surface perturbations |
| $\rho$ | fluid density |